analytical chemistry

pubs.acs.org/ac Article

Extreme Ultraviolet Photodissociation Decodes the Chain Modifications of Lipids

Yaolu Ma, Zheyi Liu, Zhixiong Jin, Heng Zhao, Jiami Zhou, Jieying Xue, Meng Zhang, Shirui Yang, Yuanjiang Pan, Weiqing Zhang, Chunlei Xiao,* Xueming Yang, and Fangjun Wang*

Cite This: https://doi.org/10.1021/acs.analchem.5c06299 Read Online

ACCESS | Metrics & More | Article Recommendations | Supporting Information

ABSTRACT: Chain modifications play critical roles in the modulation of biological functions. However, current mass spectrometry (MS) methods fall short in providing the diagnostic fragments of lipid chain modifications due to the limitations of vibrational excited fragmentations. Herein, we introduce a novel extreme ultraviolet photodissociation (EUPD), which integrates a tunable-wavelength extreme ultraviolet-free electron laser (EUV-FEL) into the MS dissociation chamber, enabling ultrafast photoexcitation and -dissociation of lipids via the dissociation pathways in electronic excited states. EUPD offers unprecedented photochemical manipulations over fragmentation patterns by tuning the EUV photon energy, enabling the highly selective cleavage of specific chemical bonds according to their different dissociation thresholds. This wavelength tunability generates rich types of diagnostic fragments for diverse lipid chain modifications, including methyl branching (95−100 nm), cyclopropane rings (100−150 nm), polyunsaturation (90−100 nm), and oxidation (140−150 nm). EUPD exhibits great potential to revolutionize MS-based lipid analysis and significantly promotes the elucidation of lipid structure−function relationships.

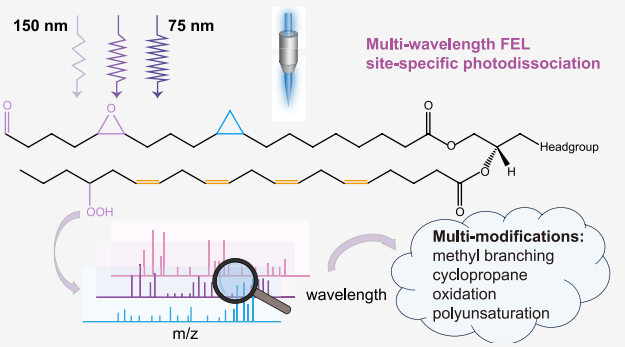

INTRODUCTION

Life utilizes a variety of modifications to precisely modulate the functions of biomolecules. Like the most famous post-translational modifications (PTMs) of proteins,[1,2] diverse chain modifications also enable the elaborate lipid functions, including cell membrane formation, signal transduction, energy storage, and sophisticated protein function regulation.[3−5] Glycerophospholipids (GPLs),[6] the most abundant structural lipids in eukaryotic membranes, are characterized by a diacylglycerol backbone linked to different head groups. The fatty acyl chains at the stereospecific numbering (*sn*)-1 and *sn*-2 positions can vary in length and saturation, contributing to the structural diversity and biophysical properties of membranes.[7,8] Distinct side-chain compositions, such as stearoyl-arachidonylglycerol (SAG) and stearoyl-oleoylglycerol (SOG), selectively recruit different protein kinase C isoforms and produce divergent downstream phosphorylation patterns. These structural differences alter lipid−protein affinities and turnover, with SAG uniquely buffering at the outer leaflet to prolong signaling duration.[9] Modifications to acyl chains, like cyclopropane modification, significantly impact GPL function and alter the survival capabilities of bacteria.[10,11] Branched chain fatty acids in dairy products are essential for mitigating inflammation, preventing cancers, and addressing metabolic disorders.[12] Furthermore, oxidized phospholipids are central mediators of inflammation and atherosclerosis, with clinical utility as biomarkers for risk prediction, reclassification, and therapeutic monitoring.[13] These diverse modifications result in complex lipid isomers, many of which occur at low abundance and yet exert strong biological effects. Therefore, precise structural elucidation—discriminating among these subtle isomeric variants—is essential for unraveling disease mechanisms and for identifying reliable biomarkers or therapeutic targets. Mass spectrometry (MS) is the central instrument of lipidomics analysis,[14,15] and the characterization of lipid structure is dependent on fragment ion profiling in tandem MS (MS/MS).[16,17] However, compared with protein PTMs, current MS-based lipid analysis pays little attention to the identification of lipid chain modifications, mainly due to the MS/MS techniques fall short in providing the diagnostic fragments of chain modifications.[18] The lack of chain modification identification severely limits our understanding of lipid structure−function relationships.

Received: October 10, 2025
Revised: December 16, 2025
Accepted: December 23, 2025
Published: December 29, 2025

Scheme 1. Schematic Representation of 75−150 nm EUPD in Decoding Diverse Chain Modifications of GPLs

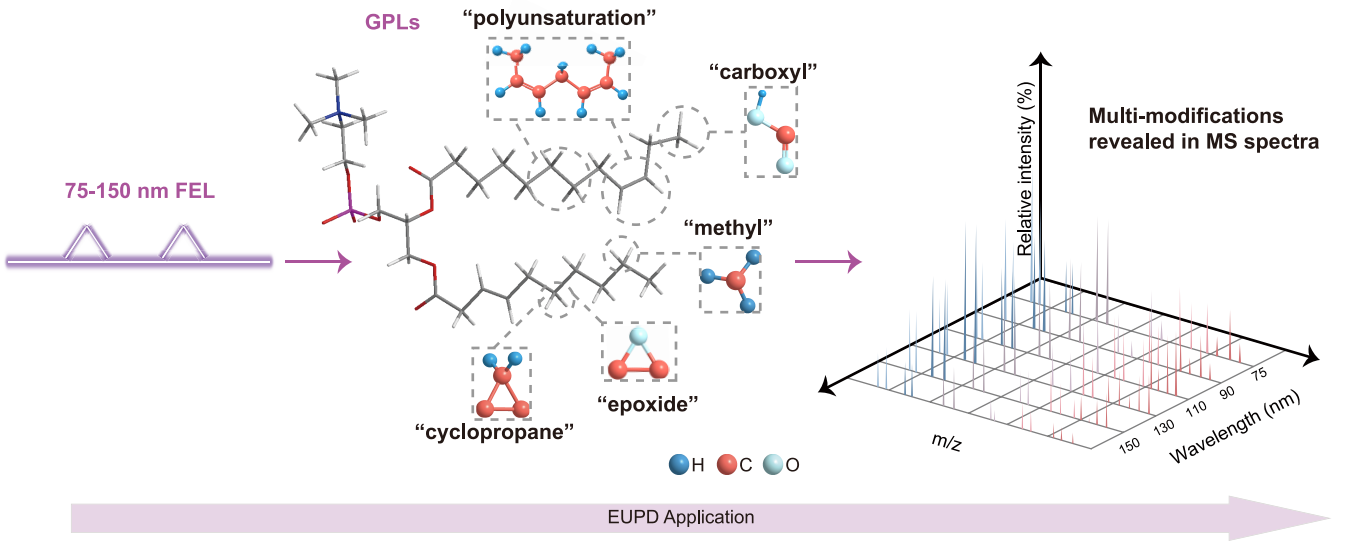

Conventional MS/MS strategies for lipid structure derivation, largely dependent on collision-induced dissociation (CID/HCD),[19] rely on the slow conversion of kinetic energy to internal vibration energy through multiple collisions with inert gas molecules (He/N_2). These methods mainly lead to lipid headgroup loss with limited fragment information regarding mostly to lipid subclass.[20] Significant progress has been made in lipid fragmentation techniques that enhance isomer resolution, ranging from gas-phase ion activation methods such as electron ionization (EI)-MS/MS CID,[21] covalent adduct chemical ionization-MS/MS CID,[22] 193/213 nm-ultraviolet photodissociation (UVPD),[23,24] ozone-induced dissociation (OzID),[25,26] electron impact excitation of ions from organics (EIEIO),[27] charge remote fragmentation (CRF),[28] and radical-directed dissociation (RDD),[29,30] to derivatization-based strategies like the Paternò−Büchi (PB) reaction.[31] These advanced MS/MS techniques provide diagnostic ions for lipid structure discrimination, thereby offering valuable frameworks for addressing the long-standing challenge of lipid isomer identification. However, despite these advances, efficient generation of adequate structure-diagnostic fragments for comprehensive lipid structure elucidation remains challenging.[32] In particular, these methods usually rely on multistage MS (e.g., MS^3 UVPD-CID) or derivatization steps that compromise detection sensitivity and increase sample complexity. Further, the processes of slower thermal activation or radical-induced pathways frequently trigger complex bond rearrangements and hydrogen scrambling, while the abundances of informative fragments of intrachain cleavages are relatively low.[32] Additionally, existing approaches remain tailored to specific modification types and require extra derivatization reaction for each modification feature, failing to simultaneous identification of multiple coexisting modifications—such as methyl branching combined with polyunsaturation or oxidation—within a single workflow. There is an urgent need to develop efficient lipid molecular scissors in MS/MS that are sufficiently sharp and fast to achieve in situ high-specificity cleavage and generation of structure feature fragments for accurate identification of diverse chain modifications.

Photoexcitation and -cleavage offer exceptional spatiotemporal precision and selectivity in biomolecular manipulation, positioning them as powerful and rapid tools for targeted chemical modifications.[33] However, conventional ultraviolet−visible photochemical reactions of biomolecules often require the introduction of specific chromophores for photon absorption and reaction initiation such as metal complex-based photocaging chemistry.[34] Currently, there is still lack of photochemical methods capable of directly targeting and manipulating different types of chemical bonds in the biomolecular skeletons. Theoretically, the photon energies in the extreme ultraviolet (EUV) range (>8 eV, <150 nm) far exceed the dissociation thresholds of single and double bonds in common biomolecules including lipids (Table S1), enabling the direct photoexcitation and -cleavage.[35] This process can promote the biomolecular skeleton into electron-excited states[36] and trigger ultrafast, bond-selective dissociation on femtosecond time scale, cleaving targeted bonds through a nonergodic mechanism before energy redistribution and potential structure rearrangement.[37,38] Unfortunately, biomolecular spectroscopy tools with EUV photon action have been lagging behind for a long time, mainly due to the absence of a tunable-wavelength EUV light source with high brightness and ultrafast pulse.[39,40]

In this study, we introduce a novel EUV photodissociation approach to decode lipid chain modifications by integrating a 75−150 nm wavelength-tunable EUV-free electron laser (EUV-FEL)[41] into the MS system. The Dalian Coherent Light Source (DCLS) beamline[42] delivered the EUV-FEL via a vacuum tube directly to the dissociation chamber of MS, enabling precise control over biomolecule photoexcitation. Lipid molecules (Table S2) were introduced into MS through electrospray ionization (ESI), and specific lipid precursor ions were selected based on their mass-to-charge (m/z) ratios. Ultrafast photoexcitation of the lipid precursor ions occurred within 1 ps using a single pulse of EUV-FEL irradiation at about 10−15 μJ/pulse. The resulting fragment ions were then detected by an Orbitrap analyzer with high mass resolution. This novel strategy, termed extreme ultraviolet photodissociation (EUPD), enabled the generation of rich types of structure-diagnostic fragment ions, revealing detailed informa-

https://doi.org/10.1021/acs.analchem.5c06299
Anal. Chem. XXXX, XXX, XXX−XXX

tion about various lipid chain modifications (Scheme 1). EUV-FEL facilitated highly selective photoactivation and -cleavage of specific bonds within lipid acyl chains by precisely tuning the wavelength (photon energy) to match the specific electronic transitions or bond dissociation thresholds, offering unprecedented photochemical manipulations over lipid fragmentation patterns.

EXPERIMENTAL SECTION

Materials

All lipid samples were purchased from Avanti Polar Lipids (Alabaster, Alabama, USA), except for 1-palmitoyl-2-(4-keto-dodec-3-ene-dioyl) phosphatidylcholine (KDdiA-PC), 1-palmitoyl-2−13(S)-HpODE-*sn*-glycero-3-phosphatidylcholine (16:0/18:2-OOH-PC), and 1-palmitoyl-2-(±)17(18)-EpETE-*sn*-glycero-3-phosphatidylcholine (EpETE-PC), which were obtained from Cayman Chemical (Ann Arbor, Michigan, USA). The chemical formulas and molecular weights of all glycerophospholipids included in this study are shown in Table S2. HPLC-grade methanol (MeOH), ethanol (EtOH), and dichloromethane (CH_2Cl_2) were purchased from Sigma-Aldrich (St. Louis, MO). The deionized water for all experiments was purified by using a Milli-Q pure water system (Millipore Inc., Milford, MA). Original lipid stock solutions (1.0 mg/mL) were prepared in a 50:50 (v/v) mixture of CH_2Cl_2 and MeOH. Then, these solutions were further diluted to a final concentration of 10 μg/mL using MeOH as the solvent.

EUPD Instrumentation

An Orbitrap Fusion Lumos Tribrid mass spectrometer (Thermo Fisher, San Jose, CA, USA) was utilized for the EUPD experiments. The experimental setup involved integrating a wavelength-tunable EUV-FEL from the DCLS beamline into the low-pressure linear ion trap (LIT) chamber through a high-vacuum tube (Figure S1). This integration required specific modifications to facilitate FEL-based EUPD: the rear cover plate of the LIT in the mass spectrometer was removed and directly connected to a custom beamline adapter, which incorporated three differential pumping systems to bridge the pressure difference between the LIT (10^{-3} Pa) and the high vacuum environment (10^{-6} Pa) of the EUV-FEL beamline, ensuring optimal experimental conditions. Considering the inherent limitations of the FEL optical path adjustment capabilities using reflective optics, the mass spectrometer was positioned on a three-dimensional adjustable vibration isolation platform to minimize any potential disturbances or vibrations during data collection. The EUV-FEL facility functions under the high-gain harmonic-generation (HGHG) mode,[43] which exploits the interaction between a seed laser and an electron beam to achieve coherent emission. The seed pulse is generated by a picosecond (ps) Ti:sapphire laser with an energy of approximately 80 μJ and a narrow spectral bandwidth spanning 240−360 nm. An electron beam, produced by a photocathode radio frequency gun, is accelerated to roughly 300 MeV using seven S-band accelerating sections, providing a bunch charge of 500 pC.[44] After being microbunched, the electron beam is directed into a radiator resonant with the nth harmonic of the seed wavelength, thereby emitting coherent FEL radiation at a wavelength of λ_{seed}/n. For the current experiments, the EUV-FEL operates at 10 Hz, producing pulses of approximately 10 μJ energy and 1 ps duration. Although our EUPD results are obtained in the EUV-FEL facility, recent advances[45,46] in compact high-harmonic-generation EUV sources suggest that EUPD might ultimately be implemented in more accessible laboratory-scale setups in the near future.

Lipid analysis involved introducing samples into the MS system equipped for static ESI via a 0.58 mm i.d. borosilicate glass emitter with a 300 nm i.d. tip, employing a platinum wire to apply a 1.2 kV ESI voltage. The MS transfer capillary temperature was maintained at 200 °C for optimal ionization. Precursor lipid ions were then selected using an isolation width of ± 0.5 m/z and directed into the dissociation chamber. A single pulse of EUV-FEL (1 ps, 10 μJ) was delivered to activate and fragment the lipid precursors within the dissociation chamber. The resulting photocleavage fragments were subsequently transferred to an Orbitrap analyzer for spectral recording. Data acquisition parameters included a resolution of 240 K, achieved by averaging 200 scans with a normalized AGC target set at 2.5E5 and a maximum injection time of 500 ms. All EUPD experiments were independently repeated at least four times to ensure reproducibility. The FEL optical path and ion beam alignment were meticulously calibrated by fine-tuning the mass spectrometer. This involved observing dissociation fragment signals from PC16:0/18:1, a test sample, to achieve the coaxial introduction of the FEL beam into the LTQ dissociation chamber.

193 nm UVPD

193 nm UVPD experiments utilized a 193 nm ArF excimer laser (Gam Laser, Orlando, FL, USA) generating single pulses of 1.5 mJ with a pulse width of 10 ns. All spectra were acquired in quadruplicate. MS/MS analysis was performed at a resolution of 240 K at 200 m/z, selecting precursor ions within a quadrupole isolation window of ± 0.5 m/z. All samples maintained a consistent normalized AGC target and maximum injection time (ms) at 2.5E5, 500.

Data Processing Methods

The data analysis pipeline combined commercial software (MSConvert[47]) for initial conversion of raw MS files to mzML format with custom R scripting for subsequent processing. Theoretical fragment ion masses, derived from the molecular formulas of lipid standards, were computed to facilitate the correlation with experimental fragment ions. Subsequent alignment of these theoretical masses with experimental data was performed within a mass tolerance of 10 ppm. Custom R scripts leveraging "tidyverse", "data.table", "mzR", and "dplyr" packages were conducted for this mass alignment and overall data analysis.

Nomenclature

Lipid structure nomenclature adheres to the guidelines established by Liebisch et al.[48] For example, the notation PC16:0/18:1 employs the X:Y format, where X indicates the total carbon atoms present within the fatty acyl chain and Y specifies the number of C═C bonds. The forward slash ("/") demarcates fatty acids with defined stereospecific numbering (sn) positions on the glycerol backbone. Double bond position, measured from the carboxyl carbon, is indicated within parentheses following the Y value.

Discrimination between the C═C bond and the cyclopropane ring utilizes the nomenclature system proposed by Blevins et al.[23] The "c" in parentheses of PC16:0/17:1(c9) denotes a cyclopropane (c) at the specific position (9) relative

https://doi.org/10.1021/acs.analchem.5c06299
Anal. Chem. XXXX, XXX, XXX−XXX

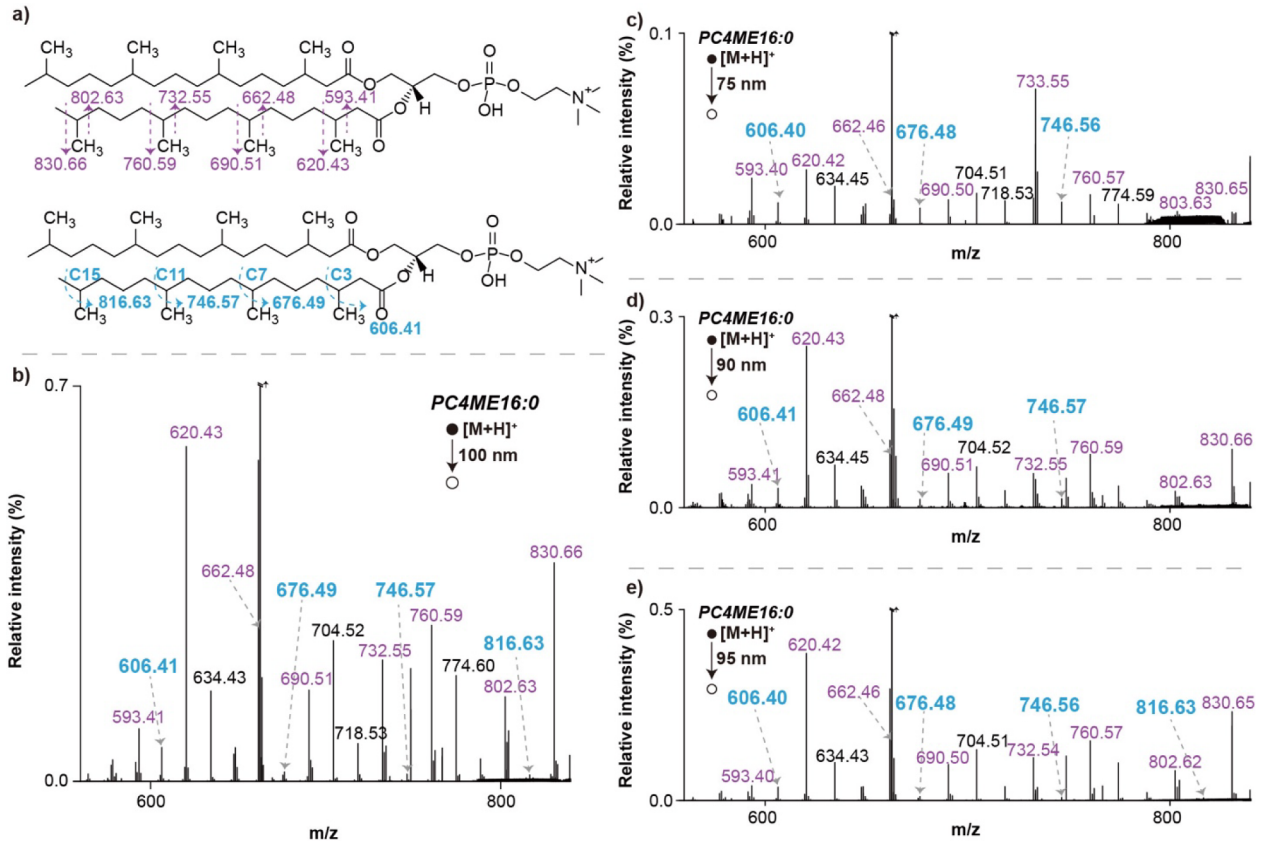

Figure 1. Discerning the polymethyl-branched structure of PC4ME16:0. (a) Proposed photocleavage sites at both backbone and branch C−C bonds of $[PC4ME16:0+H]^+$. The EUPD spectra of $[PC4ME16:0+H]^+$, m/z 846.68 at (b) 100 nm, (c) 75 nm, (d) 90 nm, and (e) 95 nm. Relative intensity normalized to precursor ion $[M + H]^+$ (%). Purple for backbone site cleavages, and blue for branch point cleavages.

to the carboxyl moiety. Abbreviations for functional groups include "Me" for a methyl branch.

RESULTS AND DISCUSSION

Tunable-Wavelength EUPD Fragmentation Pathways

The fragmentation patterns observed under EUPD are highly dependent on the laser wavelength/photon energy. The saturated-chain PC15:0 could yield an intense and evenly spaced peak envelope (CH_2, 14.02 Da), representing C−C fragmentation of the acyl chain in 75−150 nm EUV-FEL photoexcitation (Figure S2). Thus, even-electron product ions dominate the fragment spectra of saturated acyl chains. The rearrangement of hydrogen radical (H•) and subsequent elimination of a neutral alkane are commonly observed after the homolytic photocleavage of the C−C bond within saturated acyl chains.[49] On the other hand, during EUPD analysis of PC16:0/18:1, the fragment at m/z 496.34 shifts to 494.32 via losing two H atoms as the EUV-FEL wavelength decreases, indicating the formation of a carbonyl group (C═O) (Figure S3). A further H loss at the carbonyl-adjacent carbon at m/z 493.31 dominates the spectra under shorter-wavelength (90 nm) EUV-FEL irradiation. Meanwhile, fragments at m/z 577.52 and 575.50 correspond to the neutral loss of the phosphocholine headgroup from $[PC16:0/18:1+H]^+$, predominantly observed at 115 nm. When the EUV-FEL wavelength is reduced to 75 nm, this product ion shifts to m/z 576.51, suggesting radical ion formation. Similarly, the fragment at m/z 521.35 indicates a radical ion produced via the 16:0 acyl chain loss. These observations demonstrate that EUV-FEL with shorter wavelength induces high-energy, homolytic bond dissociation and favors the formation of radical fragments that remain stable in the gas phase due to the absence of collisional quenching. Additionally, the resulting odd-electron species often gain additional stability through electronic delocalization within conjugated structures, allowing for their efficient detection. Thus, EUPD minimizes the impact of backbone rearrangements on structural elucidation accuracy, thereby enhancing the reliability of lipid structure characterization.

Methyl Branching and Cyclopropane Ring

Bacterial membrane lipids such as iso- and anteiso-branched fatty acids[50] modulate membrane packing and low-temperature adaptation, while in mammals, branched-chain fatty acids derived from branched-chain amino acid metabolism accumulate in milk lipids and influence neonatal gut microbiota and immune development.[51] The polymethyl-branched phosphatidylcholine (PC), 1,2-diphytanoyl-*sn*-glycero-3-phosphocholine (PC4ME16:0), presents unique EUV photofragmentation patterns. While backbone C−C cleavage is prevalent, methyl branching points at C7, C11, and C15 (m/z 676.49, 746.57, and 816.63) are more resistant to dissociation due to the steric hindrance and electron-donating effects of methyl groups, which stabilize the adjacent C−C bonds.[21,22,52−54] This resistance is notable except for the branch site at the C3 position (m/z 606.41), where double bond conjugation upon fragmentation stabilizes the resulting ion (Figure 1a,b). Increasing photon energy enhances the ability to cleave C−C bonds and intensifies the overall fragment spectra,

https://doi.org/10.1021/acs.analchem.5c06299
Anal. Chem. XXXX, XXX, XXX−XXX

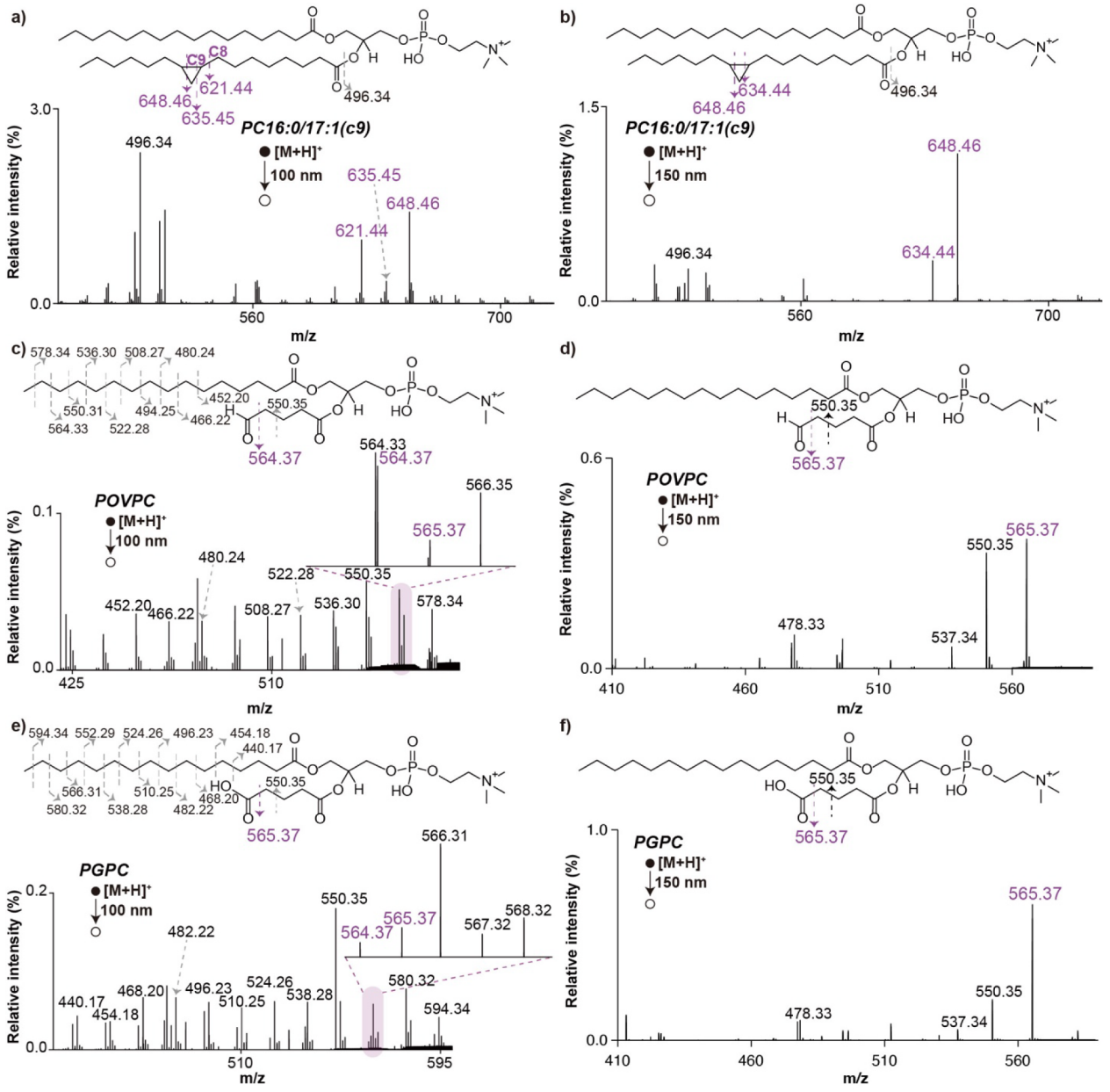

Figure 2. Discerning the cyclopropane ring and oxidation group in the acyl chains of PCs. The EUPD spectra of $[PC16:0/17:1(c9)+H]^+$, m/z 746.57 at (a) 100 nm and (b) 150 nm. The fragment ions at m/z 621.44, 634.44, 635.45, and 648.46 are generated through bond cleavages of the cyclopropane ring. The (c) 100 nm and (d) 150 nm EUPD spectra of $[POVPC+H]^+$, m/z 594.38. The (e) 100 nm and (f) 150 nm EUPD spectra of $[PGPC+H]^+$, m/z 610.37. Relative intensity normalized to precursor ion $[M + H]^+$ (%). The diagnostic fragment ion of losing the carboxyl and aldehyde groups is at m/z 565.37.

facilitating the clear distinctions between these two types of bonds. However, as photon energy reaches 16.5 eV (75 nm), the ability to discriminate between branched and straight chain C−C bonds begins to diminish. This might be attributed to the higher photon energy that can excite additional dissociation pathways at branching points that are less selective for chain modification determination. Such behavior likely reflects the redistribution of excess energy throughout the lipid molecule, thereby suppressing site-specific bond cleavage and promoting nonselective fragmentation pathways.[55,56] Consequently, the 95−100 nm photon energy range represents an optimal window that balances efficient $\sigma \rightarrow \sigma^*$ excitation/dissociation with the minimization of nonspecific dissociation channels, providing the highest selectivity for distinguishing branched versus straight-chain C−C bonds (Figure 1c−e).

Next, we investigated 1-palmitoyl-2-cis-9,10-methylenehexadecanoyl-*sn*-glycero-3-phosphocholine (PC16:0/17:1(c9)) with a cyclopropane ring at the C9 position of the *sn*-2 chain, showcasing the potential of EUPD for selective modification recognition based on tunable wavelengths. Unlike conventional collision-based methods (CID/HCD) which are difficult to provide reliable localization of cyclopropane motifs, photochemical activation can access ring-specific cleavage channels. In particular, 213 nm UVPD preferentially excites the cyclopropane unit, promoting cross-ring cleavage.[23] This cross-ring pathway cleaves both C−C bonds across the three-membered ring concurrently, yielding a diagnostic pair of

https://doi.org/10.1021/acs.analchem.5c06299
Anal. Chem. XXXX, XXX, XXX−XXX

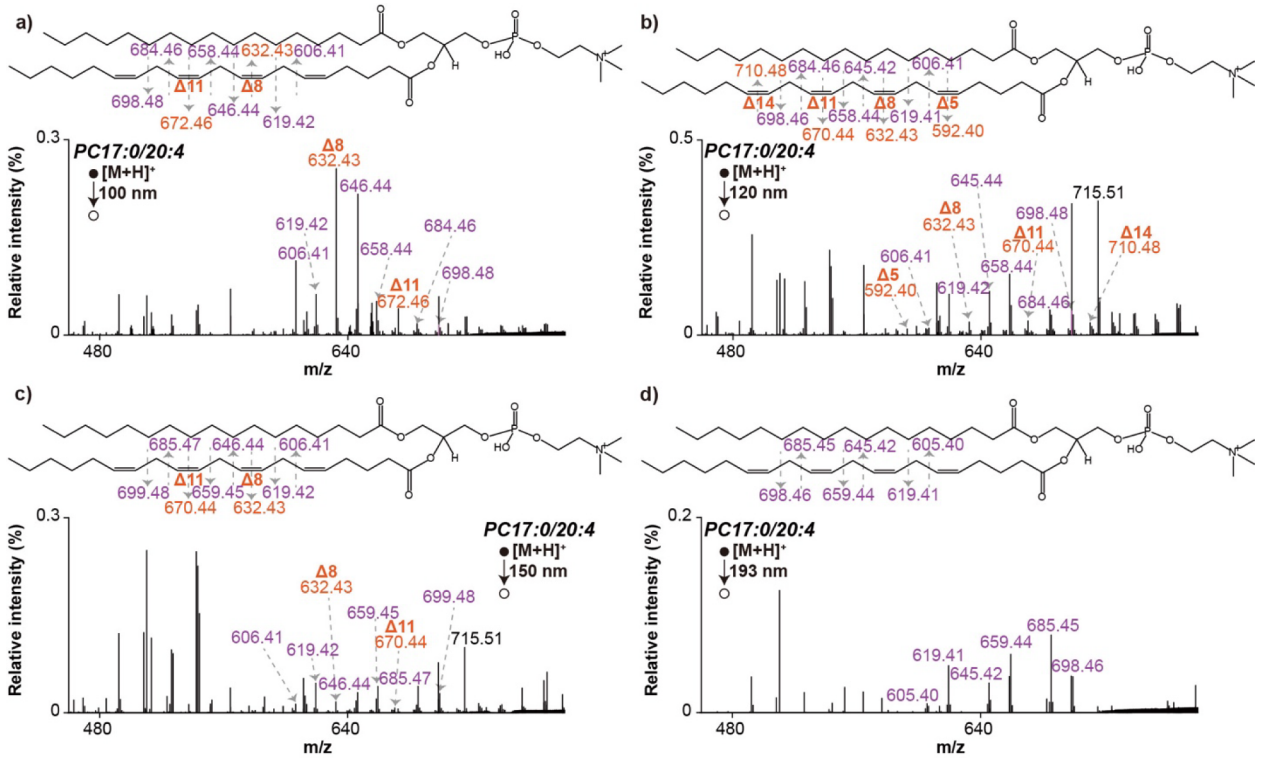

Figure 3. Polyunsaturated acyl chain fragmentation of PC17:0/20:4 (5Z, 8Z, 11Z, 14Z) upon EUPD. The fragment spectra generated by (a) 100 nm EUPD, (b) 120 nm EUPD, (c) 150 nm EUPD, and (d) 193 nm UVPD of $[PC17:0/20:4+H]^+$, m/z 796.58. Relative intensity normalized to precursor ion $[M + H]^+$ (%). Purple for C−C cleavages and orange for C═C cleavages.

fragment ions separated by a mass difference equivalent to CH_2 (14.02 Da), which is observed in the EUPD spectra as the abundant m/z 648.46/634.44 pair under long-wavelength EUV photoexcitation (e.g., 150 nm). Under shorter EUV wavelengths (e.g., 100 nm), the fragmentation pattern shifts: C8−C9 bond dissociation adjacent to the cyclopropane often predominates, producing a distinct diagnostic ion at m/z = 621.44 (Figure 2a,b). The dominating ring-opening pathway at relatively low photon energies results from the energetic favorability of relieving ring strain and forming conjugated double bonds, whereas increased photon energy enhances α-cleavage pathways that yield allylic or conjugated fragments stabilized by electronic delocalization. Collectively, photodissociation at different EUV wavelengths accesses complementary and mechanistically distinct fragmentation routes, and bond-selective EUPD channels with higher photon energy enrich the diagnostic ion palette for determining cyclopropane-modified acyl chains.

Oxidation

Oxidized phospholipids generated during oxidative stress or inflammation function as danger-associated molecular patterns, activating Toll-like receptors and shaping innate immune responses; and oxygenated derivatives of polyunsaturated fatty acids, such as prostaglandins, leukotrienes, and specialized pro-resolving mediators, orchestrate inflammation onset and resolution.[57] EUPD was employed to analyze oxidized phospholipids, including 1-palmitoyl-2-glutaryl-*sn*-glycero-3-phosphocholine (PGPC) and 1-palmitoyl-2-(5′-oxo-valeroyl)-*sn*-glycero-3-phosphocholine (POVPC), and the diagnostic fragment ions of losing the terminal carboxyl (−COOH) or aldehyde (−CHO) groups were all observed (Figure 2c−f). Intriguingly, the losses of −COOH and −CHO at the terminal end show reduced frequency when the photon energy increases, which might stem from the fundamental competition among fragmentation pathways governed by activation energy barriers. At low EUV photon energy, fragment ions resulting from terminal group losses dominate because they involve labile bonds requiring less activation energy. However, as the photon energy increases, additional pathways with higher activation energies become accessible. These include extensive C−C cleavages along the acyl chain, producing a more complex fragmentation pattern and redistributing ion abundances. Consequently, the relative intensities of simple terminal loss ions (i.e., −COOH, −CHO) are reduced due to the increased prevalence of chain scission. The fragmentation pathway upon EUPD for epoxide group is analogous to that of cyclopropane ring, as evidenced by the diagnostic fragment ions at m/z 634.444, 650.439 via the photocleavage on both adjacent sides of the oxygen atom (15.995 Da) (Figure S4). Therefore, the unique EUPD characteristics of acyl chain modifications greatly enhance the accuracy and sensitivity of lipid side-chain structure elucidation.

Polyunsaturation

The release of polyunsaturated fatty acids such as arachidonic acid from membrane phospholipids generates bioactive eicosanoids,[58] including prostaglandins and leukotrienes, which orchestrate inflammation and immune responses.[59] PC17:0/20:4 contains a polyunsaturated C20:4 (arachidonic acid) chain with double bonds at Δ5, Δ8, Δ11, and Δ14 at the *sn*-2 position. The intrinsic delocalization of the σ and π electrons renders the C═C bond less susceptible to direct bond dissociation. Therefore, 193 nm UVPD typically favors cleavage of either of the two C-C bonds adjacent to the C═C bond, producing fragments with diagnostic mass difference of

https://doi.org/10.1021/acs.analchem.5c06299
Anal. Chem. XXXX, XXX, XXX−XXX

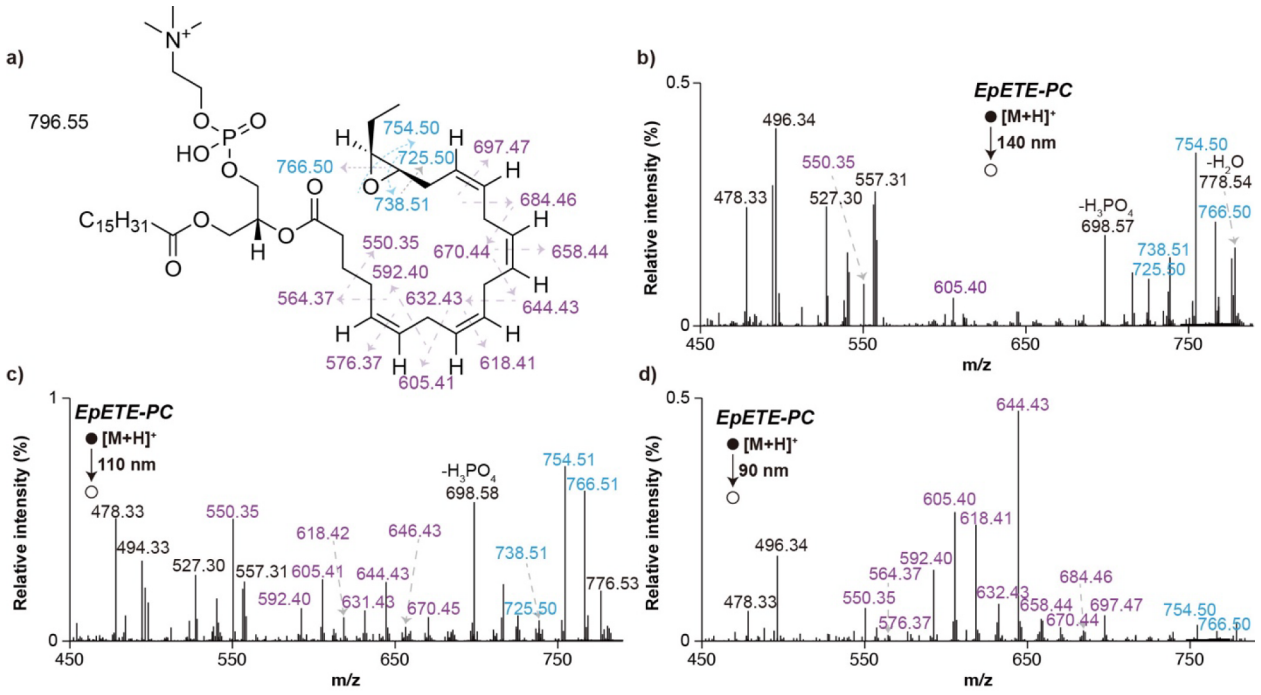

Figure 4. Discerning the polyunsaturation and epoxidation group in EpETE-PC. (a) Proposed fragmentation pathways of $[EpETE\text{-}PC+H]^+$. The (b) 140 nm, (c) 110 nm, and (d) 90 nm EUPD spectra of $[EpETE\text{-}PC+H]^+$, m/z 796.55. Relative intensity normalized to precursor ion $[M + H]^+$ (%). Purple for polyunsaturation region cleavages and blue for epoxidation group region cleavages.

24 Da.[60] However, the 24 Da facile indicator of C═C in polyunsaturated fatty acyl chains like PC17:0/20:4 becomes less discernible upon 193 nm UVPD (Figure 3d). When sufficient energy is available—such as under EUPD—$\sigma \rightarrow \sigma^*$ excitations can induce selective bond scission within the polyene system. Direct cleavage of C═C bonds is greatly enhanced along with the increase of EUV photon energy, generating C═C feature fragment ions at positions Δ5, Δ8, Δ11, and Δ14 upon 10.3 eV/120 nm. When the photon energy increases to >12.4 eV, a unique fragmentation pathway emerges, specially characterized by the highest intensity fragment ion of the C═C bond cleavage at Δ8 (m/z 632.43) and subsequent loss of $C_{12}H_{20}$ group (Figure 3a). The Δ8 C═C often shows the highest fragmentation intensity because it resides near the center of the conjugated system, where the absorbed energy tends to localize most efficiently, and its cleavage yields highly stabilized allylic or conjugated fragments. This observation suggests that EUV-FEL enables direct excitation of C═C within the polyunsaturated chain, which facilitates selective cleavage at the internal double bond positions. Other GPLs (PI, PG, and PS17:0/20:4) exhibit the same fragmentation behaviors as PC17:0/20:4 (Figures S5, S6). As a result, EUPD provides enhanced structural resolution for locating C═C positions that would otherwise be difficult to resolve by using low-energy dissociation methods.

Multiple Coexisting Modifications

To delve deeper into the characteristics of the EUPD, we further examined the fragmentation patterns of PCs bearing intricate unsaturated and oxidized acyl chains across a range of EUV photon energies. KDdiA-PC has a carboxylic acid group at the *sn*-2 chain terminus, which exhibits a propensity for photocleavage at relatively long EUV-FEL wavelengths (Figure S7a,b). The fragment ion at m/z 675.45 corresponds to the loss of the carboxylic acid group. Further, the fragments at m/z 647.42, 632.43, and 618.41 suggest the cleavage centered around the C9═O group, whereas m/z 661.43 is indicative of the direct cleavage of C10═C11 (Figure S8). On the other hand, shorter EUV-FEL wavelengths, such as 110 nm, are particularly suitable for identifying unsaturated groups due to their ability to provide sufficient energy to cleave bonds with high dissociation energies. 16:0/18:2-OOH-PC contains an *sn*-2 acyl chain bearing a conjugated diene system and a hydroperoxy group located at the C13 position (Figure S7c-e). The fragment ions observed at m/z 757.56 and 772.55 suggest the losses of hydroperoxy and hydroxyl groups, respectively. In contrast, the high-abundance fragment ion at m/z 702.47 is indicative of skeleton breakage around the C13 position. This cleavage occurs through both the C13−C14 bond and the O−O bond in the hydroperoxy group, resulting in a conjugated carbonyl and diene system at longer EUV-FEL wavelengths. Notably, when EUV photon energy reaches 13.8 eV (90 nm), the preferred fragmentation pathway yields a feature fragment at m/z 674.48 through cleavage between the C12−C13 bond, leaving the stable conjugated diene system intact (Figure S9). EpETE-PC contains an *sn*-2 polyunsaturated acyl chain with a conjugated tetraene motif and a terminal oxirane moiety (Figure 4). EUPD reveals distinct fragmentation patterns depending on the photon energy, as described above. At relatively long EUV-FEL wavelengths, the fragment spectra primarily highlight the terminal epoxide moiety, as fragment ions at m/z = 754.50 and 738.51 indicate the cleavages around the oxygen atom within this region. Conversely, higher EUV photon energies favor the identification of conjugated polyunsaturated system, and the fragments in m/z 550−700 are generated through the cleavage of C═C and C−C bonds within the *sn*-2 chain (Figure S10). These characteristics shed light on the EUV photoinduced fragmentation pathways and underlying mechanisms in decoding the structures of more sophisticated lipid molecules.

https://doi.org/10.1021/acs.analchem.5c06299
Anal. Chem. XXXX, XXX, XXX−XXX

Our results demonstrate that photochemical manipulation provides a robust and versatile approach for bond-selective activation within complex molecular systems. By coupling wavelength-tunable excitation with mass spectrometric detection, we were able to distinguish fragmentation pathways that are otherwise inaccessible through conventional collisional or thermal activation. The observed wavelength dependence of fragmentation behavior highlights the intrinsic link between electronic excitation and bond-specific reactivity. These findings not only validate the concept of wavelength-governed bond selectivity but also underscore its potential as a general strategy for structural elucidation and mechanistic studies of biomolecules. Collectively, this work establishes photochemical control as a powerful analytical and mechanistic tool for resolving subtle structural features and reaction dynamics at the molecular level.

CONCLUSION

Overall, the advent of EUPD marks a significant turning point in MS-based lipid structure elucidation. By harnessing the power of EUV wavelength tunability, picosecond ultrafast photoexcitation, bond-selective photoexcitation, and -dissociation, EUPD enables researchers to gain unprecedented insights into diverse lipid chain modifications. Its unique capacity to dissect structural features, including methyl branching, cyclopropane motifs, oxidative modifications, and polyunsaturation, offers new opportunities for elucidating lipid structure−function relationships with remarkable precision. Beyond the lipid subclasses examined in this study, the underlying potentials of EUPD can also be applied to other types of biomolecules. In ongoing work, we are assessing its utility for additional lipid categories, including sphingolipids and glycolipids as well as peptides and protein complexes. In addition to qualitative structural elucidation, EUPD also holds significant potential for quantitative lipidomics analysis. When combined with chromatographic separation and isotope labeling approaches, EUPD can globally monitor temporal lipid remodeling events and dynamic metabolic fluxes.

ASSOCIATED CONTENT

Supporting Information

The Supporting Information is available free of charge at https://pubs.acs.org/doi/10.1021/acs.analchem.5c06299.

Experimental setup details, EUPD mass spectra of additional lipids as mentioned in the text, fragmentation pathways, and tables of typical bond dissociation enthalpies and lipids used in this method (PDF)

AUTHOR INFORMATION

Corresponding Authors

Fangjun Wang − *State Key Laboratory of Chemical Reaction Dynamics, Dalian Institute of Chemical Physics, Chinese Academy of Sciences, Dalian 116023, China; University of Chinese Academy of Sciences, Beijing 100049, China;* orcid.org/0000-0002-8118-7019; Email: wangfj@dicp.ac.cn

Chunlei Xiao − *State Key Laboratory of Chemical Reaction Dynamics, Dalian Institute of Chemical Physics, Chinese Academy of Sciences, Dalian 116023, China; University of Chinese Academy of Sciences, Beijing 100049, China;* orcid.org/0000-0002-1549-5945; Email: chunleixiao@dicp.ac.cn

Authors

Yaolu Ma − *State Key Laboratory of Chemical Reaction Dynamics, Dalian Institute of Chemical Physics, Chinese Academy of Sciences, Dalian 116023, China; University of Chinese Academy of Sciences, Beijing 100049, China*

Zheyi Liu − *State Key Laboratory of Chemical Reaction Dynamics, Dalian Institute of Chemical Physics, Chinese Academy of Sciences, Dalian 116023, China; University of Chinese Academy of Sciences, Beijing 100049, China*

Zhixiong Jin − *State Key Laboratory of Chemical Reaction Dynamics, Dalian Institute of Chemical Physics, Chinese Academy of Sciences, Dalian 116023, China; Department of Chemistry, Zhejiang University, Hangzhou 310027, China*

Heng Zhao − *State Key Laboratory of Chemical Reaction Dynamics, Dalian Institute of Chemical Physics, Chinese Academy of Sciences, Dalian 116023, China*

Jiami Zhou − *Dalian Coherent Light Source, Dalian Institute of Chemical Physics, Chinese Academy of Sciences, Dalian 116023, China*

Jieying Xue − *State Key Laboratory of Chemical Reaction Dynamics, Dalian Institute of Chemical Physics, Chinese Academy of Sciences, Dalian 116023, China; University of Chinese Academy of Sciences, Beijing 100049, China*

Meng Zhang − *State Key Laboratory of Chemical Reaction Dynamics, Dalian Institute of Chemical Physics, Chinese Academy of Sciences, Dalian 116023, China*

Shirui Yang − *State Key Laboratory of Chemical Reaction Dynamics, Dalian Institute of Chemical Physics, Chinese Academy of Sciences, Dalian 116023, China; University of Chinese Academy of Sciences, Beijing 100049, China*

Yuanjiang Pan − *Department of Chemistry, Zhejiang University, Hangzhou 310027, China;* orcid.org/0000-0003-2900-2600

Weiqing Zhang − *State Key Laboratory of Chemical Reaction Dynamics, Dalian Institute of Chemical Physics, Chinese Academy of Sciences, Dalian 116023, China; University of Chinese Academy of Sciences, Beijing 100049, China; Dalian Coherent Light Source, Dalian Institute of Chemical Physics, Chinese Academy of Sciences, Dalian 116023, China;* orcid.org/0000-0001-6518-4152

Xueming Yang − *State Key Laboratory of Chemical Reaction Dynamics, Dalian Institute of Chemical Physics, Chinese Academy of Sciences, Dalian 116023, China; University of Chinese Academy of Sciences, Beijing 100049, China;* orcid.org/0000-0001-6684-9187

Complete contact information is available at: https://pubs.acs.org/10.1021/acs.analchem.5c06299

Author Contributions

F.W., C.X., and X.Y. conceived the project and designed the research. Y.M., Z.J., J.X., S.Y., and M.Z. conducted the MS analysis. C.X., Z.L., H.Z., and Z.J. performed the MS instrument construction. J.Z. and W.Z. achieved the modulation of laser wavelength and energy. Y.M. and Z.L. analyzed the data. Y.M., Z.L., Y.P., and F.W. discussed the results. Y.M. wrote the manuscript.

Notes

The authors declare no competing financial interest.

https://doi.org/10.1021/acs.analchem.5c06299
Anal. Chem. XXXX, XXX, XXX−XXX

■ ACKNOWLEDGMENTS

We thank the staff members of the Biological Mass Spectrometry System (https://cstr.cn/31127.02.DCLS.ESBMS) at the Dalian Coherent Light Source (https://cstr.cn/31127.02.DCLS) for providing technical support and assistance in data collection and analysis. This work was supported by the National Natural Science Foundation of China (grants 22525406, 92253304, and 22288201), the National Key R&D Program of China (grants 2022YFC3400502), and the Strategic Priority Research Program of the Chinese Academy of Sciences (grant XDB0450201).

■ REFERENCES

(1) Lin, Y.; Lin, P.; Lu, Y.; Zheng, J.; Zheng, Y.; Huang, X.; Zhao, X.; Cui, L. Post-Translational Modifications of RNA-Modifying Proteins in Cellular Dynamics and Disease Progression. *Adv. Sci.* **2024**, *11* (44), 2406318.
(2) Lee, J. M.; Hammarén, H. M.; Savitski, M. M.; Baek, S. H. Control of Protein Stability by Post-Translational Modifications. *Nat. Commun.* **2023**, *14* (1), 201.
(3) Levental, I.; Lyman, E. Regulation of Membrane Protein Structure and Function by Their Lipid Nano-Environment. *Nat. Rev. Mol. Cell Biol.* **2023**, *24* (2), 107−122.
(4) Coleman, R. A.; Mashek, D. G. Mammalian Triacylglycerol Metabolism: Synthesis, Lipolysis, and Signaling. *Chem. Rev.* **2011**, *111* (10), 6359−6386.
(5) Meikle, P. J.; Summers, S. A. Sphingolipids and Phospholipids in Insulin Resistance and Related Metabolic Disorders. *Nat. Rev. Endocrinol.* **2017**, *13* (2), 79−91.
(6) Hishikawa, D.; Hashidate, T.; Shimizu, T.; Shindou, H. Diversity and Function of Membrane Glycerophospholipids Generated by the Remodeling Pathway in Mammalian Cells. *J. Lipid Res.* **2014**, *55* (5), 799−807.
(7) Harayama, T.; Riezman, H. Understanding the Diversity of Membrane Lipid Composition. *Nat. Rev. Mol. Cell Biol.* **2018**, *19* (5), 281−296.
(8) Yamashita, A.; Hayashi, Y.; Nemoto-Sasaki, Y.; Ito, M.; Oka, S.; Tanikawa, T.; Waku, K.; Sugiura, T. Acyltransferases and Transacylases that Determine the Fatty Acid Composition of Glycerolipids and the Metabolism of Bioactive Lipid Mediators in Mammalian Cells and Model Organisms. *Prog. Lipid Res.* **2014**, *53*, 18−81.
(9) Schuhmacher, M.; Grasskamp, A. T.; Barahtjan, P.; Wagner, N.; Lombardot, B.; Schuhmacher, J. S.; Sala, P.; Lohmann, A.; Henry, I.; Shevchenko, A.; et al. Live-cell Lipid Biochemistry Reveals a Role of Diacylglycerol Side-chain Composition for Cellular Lipid Dynamics and Protein Affinities. *Proc. Natl. Acad. Sci. U. S. A.* **2020**, *117* (14), 7729−7738.
(10) Poger, D.; Mark, A. E. A Ring to Rule Them All: The Effect of Cyclopropane Fatty Acids on the Fluidity of Lipid Bilayers. *J. Phys. Chem. B* **2015**, *119* (17), 5487−5495.
(11) Cronan, J. E.; Luk, T. Advances in the Structural Biology, Mechanism, and Physiology of Cyclopropane Fatty Acid Modifications of Bacterial Membranes. *Microbiol. Mol. Biol. Rev.* **2022**, *86* (2), No. e00013-22.
(12) Taormina, V. M.; Unger, A. L.; Schiksnis, M. R.; Torres-Gonzalez, M.; Kraft, J. Branched-Chain Fatty Acids—An Underexplored Class of Dairy-Derived Fatty Acids. *Nutrients* **2020**, *12* (9), 2875.
(13) Tsimikas, S.; Witztum, J. L. Oxidized Phospholipids in Cardiovascular Disease. *Nat. Rev. Cardiol.* **2024**, *21* (3), 170−191.
(14) Wenk, M. R. Lipidomics: New Tools and Applications. *Cell* **2010**, *143* (6), 888−895.
(15) Bou Khalil, M.; Hou, W.; Zhou, H.; Elisma, F.; Swayne, L. A.; Blanchard, A. P.; Yao, Z.; Bennett, S. A.; Figeys, D. Lipidomics Era: Accomplishments and Challenges. *Mass Spectrom. Rev.* **2010**, *29* (6), 877−929.
(16) Yang, K.; Han, X. Lipidomics: Techniques, Applications, and Outcomes Related to Biomedical Sciences. *Trends Biochem. Sci.* **2016**, *41* (11), 954−969.
(17) Hsu, F.-F. Mass Spectrometry-based Lipidomics: An Overview. In *Mass Spectrometry-Based Lipidomics: methods and Protocols*, Hsu, F. F., ed.; Springer: New York, NY, 2021, Vol. *2306*, pp. 1−10. DOI: .
(18) Hartler, J.; Triebl, A.; Ziegl, A.; Trotzmuller, M.; Rechberger, G. N.; Zeleznik, O. A.; Zierler, K. A.; Torta, F.; Cazenave-Gassiot, A.; Wenk, M. R.; et al. Deciphering Lipid Structures Based on Platform-Independent Decision Rules. *Nat. Methods* **2017**, *14* (12), 1171−1174.
(19) McLuckey, S. A. Principles of Collisional Activation in Analytical Mass Spectrometry. *J. Am. Soc. Mass Spectrom.* **1992**, *3* (6), 599−614.
(20) Bonney, J. R.; Prentice, B. M. Perspective on Emerging Mass Spectrometry Technologies for Comprehensive Lipid Structural Elucidation. *Anal. Chem.* **2021**, *93* (16), 6311−6322.
(21) Ran-Ressler, R. R.; Lawrence, P.; Brenna, J. T. Structural Characterization of Saturated Branched Chain Fatty Acid Methyl Esters by Collisional Dissociation of Molecular Ions Generated by Electron Ionization. *J. Lipid Res.* **2012**, *53* (1), 195−203.
(22) Wang, Z.; Wang, D. H.; Park, H. G.; Tobias, H. J.; Kothapalli, K. S. D.; Brenna, J. T. Structural Identification of Monounsaturated Branched Chain Fatty Acid Methyl Esters by Combination of Electron Ionization and Covalent Adduct Chemical Ionization Tandem Mass Spectrometry. *Anal. Chem.* **2019**, *91* (23), 15147−15154.
(23) Blevins, M. S.; Klein, D. R.; Brodbelt, J. S. Localization of Cyclopropane Modifications in Bacterial Lipids via 213 nm Ultraviolet Photodissociation Mass Spectrometry. *Anal. Chem.* **2019**, *91* (10), 6820−6828.
(24) Blevins, M. S.; James, V. K.; Herrera, C. M.; Purcell, A. B.; Trent, M. S.; Brodbelt, J. S. Unsaturation Elements and Other Modifications of Phospholipids in Bacteria: New Insight from Ultraviolet Photodissociation Mass Spectrometry. *Anal. Chem.* **2020**, *92* (13), 9146−9155.
(25) Thomas, M. C.; Mitchell, T. W.; Harman, D. G.; Deeley, J. M.; Nealon, J. R.; Blanksby, S. J. Ozone-Induced Dissociation: Elucidation of Double Bond Position within Mass-Selected Lipid Ions. *Anal. Chem.* **2008**, *80* (1), 303−311.
(26) Menzel, J. P.; Young, R. S. E.; Benfield, A. H.; Scott, J. S.; Wongsomboon, P.; Cudlman, L.; Cvačka, J.; Butler, L. M.; Henriques, S. T.; Poad, B. L. J.; et al. Ozone-Enabled Fatty Acid Discovery Reveals Unexpected Diversity in the Human Lipidome. *Nat. Commun.* **2023**, *14* (1), 3940.
(27) Campbell, J. L.; Baba, T. Near-Complete Structural Characterization of Phosphatidylcholines Using Electron Impact Excitation of Ions from Organics. *Anal. Chem.* **2015**, *87* (11), 5837−5845.
(28) Wang, M.; Han, R. H.; Han, X. Fatty Acidomics: Global Analysis of Lipid Species Containing a Carboxyl Group with a Charge-Remote Fragmentation-Assisted Approach. *Anal. Chem.* **2013**, *85* (19), 9312−9320.
(29) Narreddula, V. R.; Boase, N. R.; Ailuri, R.; Marshall, D. L.; Poad, B. L. J.; Kelso, M. J.; Trevitt, A. J.; Mitchell, T. W.; Blanksby, S. J. Introduction of a Fixed-Charge, Photolabile Derivative for Enhanced Structural Elucidation of Fatty Acids. *Anal. Chem.* **2019**, *91* (15), 9901−9909.
(30) Lin, Q.; Li, P.; Jian, R.; Xia, Y. Localization of Intrachain Modifications in Bacterial Lipids Via Radical-Directed Dissociation. *J. Am. Soc. Mass Spectrom.* **2022**, *33* (4), 714−721.
(31) Ma, X.; Zhang, W.; Li, Z.; Xia, Y.; Ouyang, Z. Enabling High Structural Specificity to Lipidomics by Coupling Photochemical Derivatization with Tandem Mass Spectrometry. *Acc. Chem. Res.* **2021**, *54* (20), 3873−3882.
(32) Zhang, W.; Jian, R.; Zhao, J.; Liu, Y.; Xia, Y. Deep-lipidotyping by Mass Spectrometry: Recent Technical Advances and Applications. *J. Lipid Res.* **2022**, *63* (7), 100219.
(33) Lu, X.; Wen, Y.; Zhang, S.; Zhang, W.; Chen, Y.; Shen, Y.; Lemieux, M. J.; Campbell, R. E. Photocleavable Proteins that

https://doi.org/10.1021/acs.analchem.5c06299
Anal. Chem. XXXX, XXX, XXX−XXX

Undergo Fast and Efficient Dissociation. *Chem. Sci.* **2021**, *12* (28), 9658−9672.
(34) Liang, X.; Qian, S.; Lou, Z.; Hu, R.; Hou, Y.; Chen, P. R.; Fan, X. Near Infrared Light-Triggered Photocatalytic Decaging for Remote-Controlled Spatiotemporal Activation in Living Mice. *Angew. Chem., Int. Ed.* **2023**, *62* (48), No. e202310920.
(35) Julian, R. R. The Mechanism Behind Top-Down UVPD Experiments: Making Sense of Apparent Contradictions. *J. Am. Soc. Mass Spectrom.* **2017**, *28* (9), 1823−1826.
(36) Ashfold, M.; Cronin, B.; Devine, A.; Dixon, R.; Nix, M. The Role of $\pi\sigma^*$ Excited States in the Photodissociation of Heteroaromatic Molecules. *Science* **2006**, *312* (5780), 1637−1640.
(37) Martínez-Fernández, L.; Ranković, M. L.; Canon, F.; Nahon, L.; Giuliani, A.; Milosavljević, A. R.; Martin-Somer, A. Photodissociation of Leucine-Enkephalin Protonated Peptide: An Experimental and Theoretical Perspective. *RSC Adv.* **2024**, *14* (24), 16809−16820.
(38) Breuker, K.; Oh, H. B.; Lin, C.; Carpenter, B. K.; McLafferty, F. W. Nonergodic and Conformational Control of the Electron Capture Dissociation of Protein Cations. *Proc. Natl. Acad. Sci. U. S. A.* **2004**, *101* (39), 14011−14016.
(39) Di Mitri, S. On the Importance of Electron Beam Brightness in High Gain Free Electron Lasers. *Photonics* **2015**, *2* (2), 317−341.
(40) Canon, F.; Milosavljević, A. R.; van der Rest, G.; Réfrégiers, M.; Nahon, L.; Sarni-Manchado, P.; Cheynier, V.; Giuliani, A. Photodissociation and Dissociative Photoionization Mass Spectrometry of Proteins and Noncovalent Protein−Ligand Complexes. *Angew. Chem., Int. Ed.* **2013**, *125* (32), 8535−8539.
(41) O'Shea, P. G.; Freund, H. P. Free-Electron Lasers: Status and Applications. *Science* **2001**, *292* (5523), 1853−1858.
(42) Wang, D. An Overview of Light Source Development in Asia. In *Proceedingsof IPAC2013, FRYAA01*; JACoW, 2013; p. 4006.
(43) Yu, L. H.; Babzien, M.; Ben-Zvi, I.; DiMauro, L. F.; Doyuran, A.; Graves, W.; Johnson, E.; Krinsky, S.; Malone, R.; Pogorelsky, I.; et al. High-Gain Harmonic-Generation Free-Electron Laser. *Science* **2000**, *289* (5481), 932−934.
(44) Zhou, J.; Zhao, Y.; Hansen, C. S.; Yang, J.; Chang, Y.; Yu, Y.; Cheng, G.; Chen, Z.; He, Z.; Yu, S.; et al. Ultraviolet Photolysis of H2S and its Implications for SH Radical Production in the Interstellar Medium. *Nat. Commun.* **2020**, *11*, 1547.
(45) Han, S.; Kim, H.; Kim, Y. W.; Kim, Y.-J.; Kim, S.; Park, I.-Y.; Kim, S.-W. High-Harmonic Generation by Field Enhanced Femtosecond Pulses in Metal-Sapphire Nanostructure. *Nat. Commun.* **2016**, *7* (1), 13105.
(46) Li, R.; Xu, H.; Li, K.; Zhang, G.; Niu, J.; Tang, J.; Xu, Z.; Xiao, Y.; Guo, X.; Hu, J.; et al. Development of a Table-Top High-Power, High-Stability, High-Harmonic-Generation Extreme-Ultraviolet Laser Source. *Photonics* **2025**, *12* (9), 942.
(47) Chambers, M. C.; Maclean, B.; Burke, R.; Amodei, D.; Ruderman, D. L.; Neumann, S.; Gatto, L.; Fischer, B.; Pratt, B.; Egertson, J.; et al. A cross-platform toolkit for mass spectrometry and proteomics. *Nat. Biotechnol.* **2012**, *30* (10), 918−920.
(48) Liebisch, G.; Vizcaíno, J. A.; Köfeler, H.; Trötzmüller, M.; Griffiths, W. J.; Schmitz, G.; Spener, F.; Wakelam, M. J. O. Shorthand Notation for Lipid Structures Derived from Mass Spectrometry. *J. Lipid Res.* **2013**, *54* (6), 1523−1530.
(49) Waschewsky, G. C. G.; Kitchen, D. C.; Browning, P. W.; Butler, L. J. Competing Bond Fission and Molecular Elimination Channels in the Photodissociation of CH3NH2 at 222 nm. *J. Phys. Chem.* **1995**, *99* (9), 2635−2645.
(50) Kaneda, T. Iso- and Anteiso-fatty Acids in Bacteria: Biosynthesis, Function, and Taxonomic Significance. *Microbiol. Rev.* **1991**, *55* (2), 288−302.
(51) Ran-Ressler, R. R.; Devapatla, S.; Lawrence, P.; Brenna, J. T. Branched Chain Fatty Acids Are Constituents of the Normal Healthy Newborn Gastrointestinal Tract. *Pediatr. Res.* **2008**, *64* (6), 605−609.
(52) Alabugin, I. V.; dos Passos Gomes, G.; Abdo, M. A. Hyperconjugation. *WIREs Comput. Mol. Sci.* **2019**, *9* (2), No. e1389.
(53) Izgorodina, E. I.; Coote, M. L.; Radom, L. Trends in R−X Bond Dissociation Energies (R = Me, Et, i-Pr, t-Bu; X = H, CH3, OCH3, OH, F): A Surprising Shortcoming of Density Functional Theory. *J. Phys. Chem. A* **2005**, *109* (33), 7558−7566.
(54) Korth, H.-G.; Sicking, W. Prediction of Methyl C−H Bond Dissociation Energies by Density Functional Theory Calculations. *J. Chem. Soc., Perkin Trans. 2* **1997**, No. 4, 715−720.
(55) Murphy, B. F.; Osipov, T.; Jurek, Z.; Fang, L.; Son, S. K.; Mucke, M.; Eland, J. H. D.; Zhaunerchyk, V.; Feifel, R.; Avaldi, L.; et al. Femtosecond X-Ray-Induced Explosion of C60 at Extreme Intensity. *Nat. Commun.* **2014**, *5* (1), 4281.
(56) Boll, R.; Schäfer, J. M.; Richard, B.; Fehre, K.; Kastirke, G.; Jurek, Z.; Schöffler, M. S.; Abdullah, M. M.; Anders, N.; Baumann, T. M.; et al. X-ray Multiphoton-Induced Coulomb Explosion Images Complex Single Molecules. *Nat. Phys.* **2022**, *18* (4), 423−428.
(57) Mauerhofer, C.; Philippova, M.; Oskolkova, O. V.; Bochkov, V. N. Hormetic and Anti-inflammatory Properties of Oxidized Phospholipids. *Mol. Aspects Med.* **2016**, *49*, 78−90.
(58) Biernacki, M.; Skrzydlewska, E. Metabolic Pathways of Eicosanoids—Derivatives of Arachidonic Acid and Their Significance in Skin. *Cell. Mol. Biol. Lett.* **2025**, *30* (1), 7.
(59) Dyall, S. C.; Balas, L.; Bazan, N. G.; Brenna, J. T.; Chiang, N.; da Costa Souza, F.; Dalli, J.; Durand, T.; Galano, J.-M.; Lein, P. J.; et al. Polyunsaturated Fatty Acids and Fatty Acid-derived Lipid Mediators: Recent Advances in the Understanding of Their Biosynthesis, Structures, and Functions. *Prog. Lipid Res.* **2022**, *86*, 101165.
(60) Williams, P. E.; Klein, D. R.; Greer, S. M.; Brodbelt, J. S. Pinpointing Double Bond and Sn-Positions in Glycerophospholipids via Hybrid 193 nm Ultraviolet Photodissociation (UVPD) Mass Spectrometry. *J. Am. Chem. Soc.* **2017**, *139* (44), 15681−15690.

NOTE ADDED AFTER ASAP PUBLICATION

This paper was published ASAP on December 29, 2025, with typographical errors in the TOC/abstract and Scheme 1. The corrected version was reposted on January 6, 2026.

https://doi.org/10.1021/acs.analchem.5c06299
Anal. Chem. XXXX, XXX, XXX−XXX